Membrane-adhesion-induced phase separation of two species of junctions

Jia-Yuan Wu[1,2] and Hsuan-Yi Chen[1,2,3]
[1]*Department of Physics, National Central University, Jhongli 32054, Taiwan*
[2]*Center for Complex Systems, National Central University, Jhongli 32054, Taiwan*
[3]*Graduate Institute of Biophysics, National Central University, Jhongli 32054, Taiwan*
(Received 15 September 2005; revised manuscript received 27 October 2005; published 24 January 2006)

A theory of membrane-adhesion-induced phase separation of two species of ligand-receptor complexes (i.e., junctions) is presented. Different species of junctions are assumed to have different natural heights and flexibilities. It is shown that the equilibrium properties of the system are equivalent to a membrane under an effective external potential, and for given junction flexibility difference phase separation occurs at sufficiently large junction height difference. The phase coexistence curve shows two distinct regions. (i) When junction height difference is large, the system is far from the mean-field critical point. Because of the higher entropy associated with softer junctions, phase coexistence occurs when the harder junctions have higher effective binding energy (free energy released due to the formation of a junction). (ii) When junction height difference is small such that the system is near the mean-field critical point, the contribution of the binding energy of the softer junctions to the free energy of the state with intermembrane distance close to the natural height of the harder junctions is not negligible. Therefore phase coexistence occurs when the harder junctions have smaller effective binding energy. Monte Carlo simulation that studies the effect of non-Gaussian fluctuations on the critical point indicates that the situation described in (ii) can be observed in typical biological systems.

DOI: 10.1103/PhysRevE.73.011914 PACS number(s): 87.16.Dg, 68.05.−n, 64.60.−i

I. INTRODUCTION

The physics of membrane adhesion [1] has attracted attention from both experimentalists and theorists in recent years [2–10]. Membrane adhesions are often mediated by more than one type of lock-and-key molecular complexes (in the rest of this article, these complexes are called junctions for simplicity). A celebrated example is the formation of an immunological synapse between a T cell and an antigen-present cell (APC), a key event governing a mature immune response. [11] When a T lymphocyte interacts with an APC, a patch of target-patterned membrane adhesion region forms between them, where the TCR/MHC-peptide complexes aggregate in the center where a LFA-1/ICAM-1 complex-rich region surrounds it. This and other types of membrane-adhesion-induced phase separation of two species of junctions have been a topic of considerable research interest [12–14]. Qi *et al.* [12] developed a set of coarse-grained reaction-diffusion equations to model the dynamics of immunological synapse pattern formation. Their study qualitatively agrees with experiments [11] and suggests that, because of the height difference between the two species of junctions, there is a phase separation of different types of junctions induced by membrane adhesion, and the formation of a target-patterned immunological synapse is a natural result of this phase separation. Although recent Monte Carlo simulation of Weikl and Lipowsky [14] shows that the height difference between different types of junctions only drives a phase separation, and the formation of a target-patterned immunological synapse has to be assisted by the cytoskeleton, there is no doubt that statistical physics plays a major role in clarifying the underlying mechanism of membrane adhesion mediated by multiple species of junctions.

Besides the study of the dynamics of immunological synapse formation, equilibrium statistical mechanics and thermodynamics also provide much information on membrane-adhesion-induced phase separation of multiple species of junctions. For example, one of us [15] has developed an equilibrium statistical mechanical analysis which provides a phase diagram for such systems on the mean field level. The effects of membrane height fluctuations were also studied by a one-loop calculation in [15], and the result shows that membrane height fluctuations not only renormalize the binding energy of the junctions but also induce effective interactions between the junctions. Another recently developed equilibrium macroscopic theory by Coombs *et al.* [16] that basically extends the classical work of Bell [17] to the case of the T cell/APC system provides criteria for the formation of target-patterned immunological synapses by line-tension considerations. An interesting work by Raychaudhuri *et al.* [18] reduces the reaction-diffusion equations in [12] to an effective membrane model, and the condition for forming an immunological synapse is studied by the mean field, Gaussian, and renormalization group theories.

In this article, we reexamine the system studied in [15] with an effective membrane model that is closely related to [18]. Instead of focusing on the T cell-APC system as Ref. [18] does, we are interested in the general case of two membranes binding to each other due to the presence of two junctions types. Our aim is to provide the equilibrium phase diagram for this type of system by including the effects of junction height difference, junction flexibility difference, and thermally activated membrane height fluctuations. In Sec. II, we introduce our model Hamiltonian. By summing over all possible junction distributions, an effective membrane model with only one fluctuating variable, i.e., the intermembrane distance, is obtained. In this model the specific ligand-receptor interactions are replaced by an effective intermembrane potential that comes from the thermal average of junction-induced interactions between the membranes. In

Sec. III we study the phase diagram of this system in the mean field level. In this simple analysis the equilibrium intermembrane distance is located at the minimum of the effective intermembrane potential, and phase coexistence occurs when the effective intermembrane potential has two degenerate minimums. Our analysis shows that the mean field model of the effective intermembrane potential approach is equivalent to the hard membrane solution of [15], in which the analysis is done by deriving the effective interjunction interactions by neglecting membrane height fluctuations. In Sec. IV we apply Gaussian approximation to study the effect of membrane height fluctuations on the phase diagram for the case when two species of intermembrane junctions have different flexibilities. We find that the phase coexistence curve shows two distinct regions. The first region is when junction height difference is sufficiently large such that there is no type-α junctions in the type-β-junction-rich domain ($\alpha \neq \beta$). In this case phase coexistence occurs when the harder junctions have higher effective binding energy (effective binding energy is the free energy released by the system when a free ligand and a free receptor form a junction) because the harder junctions have less entropy than the softer junctions. The second region is when the junction height difference is not very large such that the system is in the two-phase region close to the mean field critical point. In this case the density of the softer junctions in the state where intermembrane distance is close to the natural height of the harder junctions is not negligible because they can be stretched or compressed easily. As a result the effective binding energy of the softer junctions lowers the free energy of the state with intermembrane distance close to the harder junctions, therefore phase coexistence occurs when the effective binding energy of the harder junctions is smaller than that of the softer junctions. Section V discusses possible effects of non-Gaussian fluctuations with Monte Carlo simulations and summarizes this work.

II. THE MODEL

The system that we study in this article is shown schematically in Fig. 1. Two species of ligand-receptor pairs bind two membranes together. The heights of the membranes measured from the reference plane (i.e., the xy plane) are denoted by $z_1(\mathbf{r})$ and $z_2(\mathbf{r})$, respectively, where $\mathbf{r}=(x,y)$ is a two-dimensional planar vector. There are two types of anchored receptors in membrane 1 and two types of anchored ligands in membrane 2. Type-α receptors (α is 1 or 2) form specific lock-and-key complexes with type-α ligands. These are reversible, noncovalent bonds. The density of type-α junctions at $\mathbf{r}$ is $\Phi_\alpha(\mathbf{r})$, and the densities of free type-α receptors and ligands at $\mathbf{r}$ are $\Psi_{R\alpha}(\mathbf{r})$ and $\Psi_{L\alpha}(\mathbf{r})$, respectively. The binding energy of a type-α junction is denoted by $E_{B\alpha}$. Choosing the energy unit to be k_BT, the effective Hamiltonian of the system in the mesoscopic scale where the continuum theory of membrane elasticity is applicable has the following form:

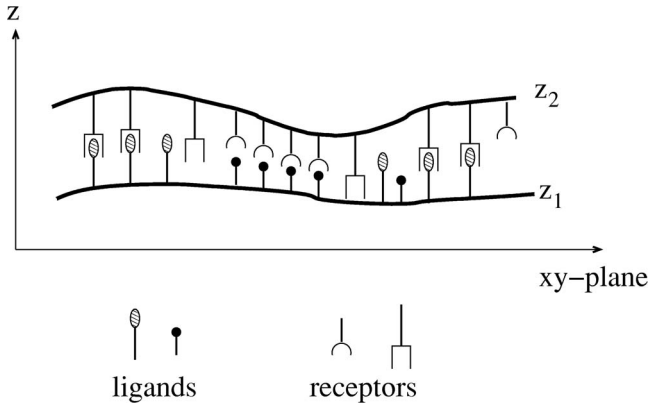

FIG. 1. Schematics of the system. Two species of ligand-receptor pairs bind two membranes together. The heights of the membranes measured from the reference plane (i.e., the xy plane) are $z_1(\mathbf{r})$ and $z_2(\mathbf{r})$, respectively, where $\mathbf{r}=(x,y)$ is a two-dimensional planar vector. There are two types of anchored receptors in membrane 1 and two types of anchored ligands in membrane 2. Type-α receptors (α is 1 or 2) form specific lock-and-key complexes with type-α ligands. They have different natural lengths h_1 and h_2. In general, different types of junctions also have different flexibilities. The softer junctions are easier to be stretched or compressed from their natural length than the harder junctions.

$$H = \int d^2r \left(\frac{\kappa}{2}[\nabla^2 h(\mathbf{r})]^2 + \frac{\gamma}{2}[\nabla h(\mathbf{r})]^2 + \sum_{\alpha=1}^{2} \frac{\lambda_\alpha}{2} \Phi_\alpha(\mathbf{r})[h(\mathbf{r}) - h_\alpha]^2 - \sum_{\alpha=1}^{2} \Phi_\alpha(\mathbf{r}) E_{B\alpha} \right). \quad (1)$$

Here $h(\mathbf{r})=z_1(\mathbf{r})-z_2(\mathbf{r})$ is the intermembrane distance at $\mathbf{r}$. The first and second terms on the right-hand side are the bending elastic energy and surface tension of the membranes. κ is related to the bending modulus of the membranes by $\kappa=\kappa_1\kappa_2/(\kappa_1+\kappa_2)$ [20], and γ is related to the surface tensions of the membranes by $\gamma=\gamma_1\gamma_2/(\gamma_1+\gamma_2)$ [20]. For simplicity we have neglected the possible dependence of κ and γ on the densities of the receptors and ligands anchored in the membranes. We assume that in the presence of a type-α junction, the interaction energy between the membranes acquires a minimum at $h=h_\alpha$ (the natural length of a type-α junction), and the coupling term $\Sigma_{\alpha=1}^2(\lambda_\alpha/2)\Phi_\alpha(\mathbf{r}) \times[h(\mathbf{r})-h_\alpha]^2$ comes from the Taylor expansion around this minimum. Here λ_α is the flexibility of a type-α junction against stretch and compression. The last term on the right-hand side is the binding energy between the receptors and the ligands. Typical values of material parameters mentioned above are listed in Table I. To focus on the effects of membrane and junction elasticity, the direct interactions between the receptors, ligands, and junctions have been neglected in this model. For the same reason, the nonspecific interactions between the membranes are also neglected, except for the constraint $h>0$, i.e., the membranes cannot cross each other. We further choose the unit length in the xy plane to be $a \sim 6$ nm, the smallest length scale for the continuum elasticity theory of membranes to be valid [22], and the unit length in

TABLE I. Typical values of material parameters.

Parameter	Symbol	Typical value
Bending rigidity	κ	$2-70\times10^{-20}$ N m [2]
Surface tension	γ	24×10^{-6} N/m [21]
Junction elastic constant	λ_α	$10-10^6\times10^{-6}$ N/m [17]
Junction length	h_α	10–30 nm [17]
Junction binding energy	$E_{B\alpha}$	$10k_BT$
Number of receptors	$N_{R\alpha}$	10^5/cell [17]
Number of ligands	$N_{L\alpha}$	10^5/cell [17]
Surface area of cells	A_C	$10-10^4$ μm^2

the z direction is chosen to be $\sqrt{a^2k_BT/\kappa}=\sqrt{a^2/\kappa}\equiv l_0$. Thus the Hamiltonian of the system can be expressed in the nondimensional form,

$$H_{cont}=\int d^2r\left(\frac{1}{2}[\nabla^2 l(\mathbf{r})]^2+\frac{\Gamma}{2}[\nabla l(\mathbf{r})]^2+\sum_{\alpha=1}^{2}\frac{\Lambda_\alpha}{2}\phi_\alpha(\mathbf{r})[l(\mathbf{r})-l_\alpha]^2-\sum_{\alpha=1}^{2}\phi_\alpha E_{B\alpha}\right), \quad (2)$$

where $l=h/l_0$ is the dimensionless intermembrane distance, $l_\alpha=h_\alpha/l_0$ is the dimensionless natural length of type-α junction, $\phi_\alpha=a^2\Phi_\alpha$ is the dimensionless junction density, $\Gamma=\gamma l_0^2$ is the dimensionless surface tension, $\Lambda_\alpha=\lambda_\alpha l_0^2$ is the dimensionless junction flexibility, and all in-plane lengths and heights are scaled by a and l_0, respectively.

Our analysis is performed on a two-dimensional square lattice with $L^2=N$ sites and lattice constant a. Therefore, we shall proceed with our discussion with the discrete version of Eq. (2),

$$H_{lat}=\sum_{i,j=1}^{L}\left[\frac{1}{2}[\Delta_d l(i,j)]^2+\frac{\Gamma}{2}[\nabla l(i,j)]^2+\sum_{\alpha=1}^{2}\phi_\alpha(i,j)\left(\frac{\Lambda_\alpha}{2}[l(i,j)-l_\alpha]^2-E_{B\alpha}\right)\right], \quad (3)$$

where the discrete Laplacian of l is given by $\Delta_d l(i,j)=l(i+1,j)+l(i-1,j)+l(i,j-1)+l(i,j+1)-4l(i,j)$, and the discrete gradient of l is $\nabla l(i,j)=\frac{1}{2}\{[l(i+1,j)-l(i-1,j)]\hat{\mathbf{x}}+[l(i,j+1)-l(i,j-1)]\hat{\mathbf{y}}\}$.

The partition function of this system can be expressed as integrals over all possible membrane height and junction distributions under the condition that the free ligands, free receptors, and junctions have reached chemical equilibrium. When the densities of free ligands and free receptors are small, it is convenient to define the effective binding energy of the junctions,

$$e^{E_{B\alpha}+\mu_\alpha}=\psi_{R\alpha}\psi_{L\alpha}e^{E_{B\alpha}}=e^{E_{eff\,\alpha}}, \quad (4)$$

where μ_α is the chemical potential of type-α junctions, and $\psi_{R\alpha}$ and $\psi_{L\alpha}$ are the dimensionless type-α receptor and ligand density, respectively. The effective binding energy can be intuitively understood as the free energy released by the system due to the formation of a junction. Higher value of $E_{eff\,\alpha}$ means higher tendency for the formation of type-α junctions. We assume that each site can be occupied by lipids, or one type-1 junction, or one type-2 junction, therefore our analysis is carried out in grand canonical ensemble. [19] After summing over all possible distributions of the junctions, the partition function can be expressed as

$$Z=\int \mathcal{D}[l]e^{-H_{el}[l]}\prod_{i,j=1}^{L}\left[1+\exp\left(E_{eff\,1}-\frac{\Lambda_1}{2}[l(i,j)-l_1]^2\right)+\exp\left(E_{eff\,2}-\frac{\Lambda_2}{2}[l(i,j)-l_2]^2\right)\right] \quad (5)$$

$$=\int \mathcal{D}[l]\exp\left[-\left(H_{el}+\sum_{i,j=1}^{L}V_{eff}[l(i,j)]\right)\right] \quad (6)$$

where

$$H_{el}=\sum_{i,j=1}^{L}\left(\frac{1}{2}[\Delta_d l(i,j)]^2+\frac{\Gamma}{2}[\nabla l(i,j)]^2\right), \quad (7)$$

and

$$V_{eff}(l)=-\ln\left[1+\sum_{\alpha=1}^{2}\exp\left(E_{eff\,\alpha}-\frac{\Lambda_\alpha}{2}(l-l_\alpha)^2\right)\right]. \quad (8)$$

That is, after summing over all possible junction distributions, the partition function becomes the same as that of a membrane with height $l(i,j)$ under an effective potential $V_{eff}(l)$. It is important to point out that although the effective potential approach is apparently similar to Ref. [18], the basic idea behind the current approach is actually more closely related to the series of studies carried out in Refs. [6,7,23]. Reference [18] begins with reaction-diffusion equations for the system, in the limit when binding and unbinding of ligand-receptor pairs are fast; the dynamics of the membrane height in this system is shown to be equivalent to that of a membrane under an effective external potential. On the other hand, we study the equilibrium properties of the system; the effective potential is a result of summing over all junction distributions in a grand partition function. This is closer to Refs. [6,7,23], where generic interactions, repellers, and reversible stickers between a membrane and a substrate is considered, and the equilibrium properties of the system are studied by first summing over the degrees of freedom associated with the repellers and stickers; after this step the system becomes equivalent to a membrane under an effective potential. The membrane height is then studied either by analytical approximation or by Monte Carlo simulations. Our potentials and the effective potentials in Refs. [6,7,23] all arise as a result of partial summation of the grand partition function. The validity of this approach in equilibrium is independent of the time scales of junction binding and unbinding. Of course, therefore our study does not provide information about the dynamics of the system.

Typical experimental systems (either in living cells or artificial membranes) are not open systems that exchange ligands and receptors with the environment. Instead, the total

numbers of ligands and receptors in the system are often, to a good approximation, fixed. To compare our analysis with experiments, notice that the total number of type-α junctions, N_α, in the system can be expressed as the derivative of the grand potential with respect to its effective binding energy because

$$G = -\ln Z$$

and

$$N_\alpha = -\frac{\partial G}{\partial \mu_\alpha} = -\frac{\partial G}{\partial E_{eff\,\alpha}} = \sum_{i,j} \left\langle \frac{\exp\left(E_{eff\,\alpha} - \frac{\Lambda_\alpha}{2}[l(i,j) - l_\alpha]^2\right)}{1 + \sum_\beta \exp\left(E_{eff\,\beta} - \frac{\Lambda_\beta}{2}[l(i,j) - l_\beta]^2\right)} \right\rangle, \tag{9}$$

and $N_{R\alpha}$ ($N_{L\alpha}$), the total number of type α receptors (ligands) in the system, can be calculated by adding the total number of free type-α receptors (ligands) to the total number of type-α junctions. For example,

$$N_{R\alpha} = A_C \psi_{R\alpha} + N \psi_{R\alpha} \psi_{L\alpha} \times e^{E_{B\alpha}} \left\langle \frac{\exp\left(-\frac{\Lambda_\alpha}{2}(l - l_\alpha)^2\right)}{1 + \sum_\beta \psi_{R\beta}\psi_{L\beta} \exp\left(E_{B\beta} - \frac{\lambda_\beta}{2}(l - l_\beta)^2\right)} \right\rangle, \tag{10}$$

where A_C is the area of the cell membrane in which type-α receptors are anchored. Typical values of the effective binding energies can be estimated in the following way. Typical values for $N_{R\alpha}$ and $N_{L\alpha}$ are on the order of 10^5 per cell. Although $A_C\psi_{R\alpha}$ and $A_C\psi_{L\alpha}$ (total number of free type-α receptors and ligands) are smaller than $N_{R\alpha}$ and $N_{L\alpha}$, we expect them to be of the same order as $N_{R\alpha}$ and $N_{L\alpha}$ except in some extreme cases where almost all of the receptors and ligands become junctions in the adhesion zone. Therefore from $A_C \sim 10$–10^4 μm^2, we find that typical values of $\psi_{R\alpha}$ and $\psi_{L\alpha}$ should be $\psi_{R\alpha(L\alpha)} \leqslant \mathcal{O}(10^{-2})$. With typical binding energy $E_{B\alpha} \sim 10$–20, typical values of $E_{eff\,1}$ and $E_{eff\,2}$ should be of order unity, and they can be positive or negative. In the rest of this article, we shall choose the effective binding energies within this range such that the parameters correspond to typical experimental systems.

III. EFFECTIVE MEMBRANE POTENTIAL AND MEAN FIELD THEORY

Let us neglect membrane height fluctuations and assume that the membranes are flat for a moment. In this mean field approximation the equilibrium value of $l(i,j)$ is simply determined by minimizing V_{eff}. In order to proceed with our discussion in a more systematic way, we further define $\Lambda_\pm = \Lambda_1 \pm \Lambda_2$, $E_{eff_\pm} = E_{eff\,1} \pm E_{eff\,2}$, $l_a = (l_1 + l_2)/2$, $\Delta_h = (l_2 - l_1)/2$, $\lambda = \Lambda_-/\Lambda_+$, and $g = \Delta_h^2 \Lambda_+$. These parameters are listed in Table II. Substituting these parameters in Eq. (8), one finds that

TABLE II. Dimensionless parameters introduced in the text.

$l_a = l_1 + l_2/2$
$\Delta_h = l_2 - l_1/2$
$\Lambda_\pm = \Lambda_1 \pm \Lambda_2$
$\lambda = \Lambda_-/\Lambda_+$
$g = \Delta_h^2 \Lambda_+$
$E_{eff\,\pm} = E_{eff\,1} \pm E_{eff\,2}$

$$V_{eff}(l) = -\ln\left\{1 + \exp\left(\frac{E_{eff_+} - g/2}{2}\right) A(z)\right\}, \tag{11}$$

where

$$A(z) = \exp\left(\frac{E_{eff_-} - g\lambda/2}{2} - g\frac{1+\lambda}{4}[(z+1)^2 - 1]\right) + \exp\left(-\frac{E_{eff_-} - g\lambda/2}{2} - g\frac{1-\lambda}{4}[(z-1)^2 - 1]\right), \tag{12}$$

and $z = (l - l_a)/\Delta_h$. The equilibrium membrane height is determined by the condition

$$\frac{dV_{eff}}{dz} = -\frac{\exp\left(\frac{E_{eff_+} - g/2}{2}\right)}{1 + \exp\left(\frac{E_{eff_+} - g/2}{2}\right) A(z)} \frac{dA(z)}{dz} = 0; \tag{13}$$

therefore the equilibrium value of z is a root of $dA(z)/dz = 0$, and it is independent of E_{eff_+}. The fact that the phase boundary in the mean field theory is independent of the sum of the effective binding energies of the junctions, E_{eff_+}, and only depends on λ, g, and E_{eff_-} is an artifact that only holds in the mean field theory. When we include membrane fluctuations by Gaussian approximation in the next section, the resulting phase boundary does depend on E_{eff_+}.

When $\lambda = 0$, both types of junctions have the same flexibility, and

$$A(z) = \exp\left(\frac{E_{eff_-}}{2} - \frac{g}{4}[(z+1)^2 - 1]\right) + \exp\left(-\frac{E_{eff_-}}{2} - \frac{g}{4}[(z-1)^2 - 1]\right). \tag{14}$$

In this case, the phase boundary in the gE_{eff_-} plane is located at the E_{eff_-} axis. Straightforward calculation leads to the critical point ($E_{eff_-} = 0$, $g = 2$). When $g < 2$, there is a triple root for $dA(z)/dz = 0$ at $z = 0$ which corresponds to $l(i,j) = l_a$ at all lattice sites. The physical picture of this case is clear: when both types of junctions have the same flexibility against stretch and compression, phase separation is driven

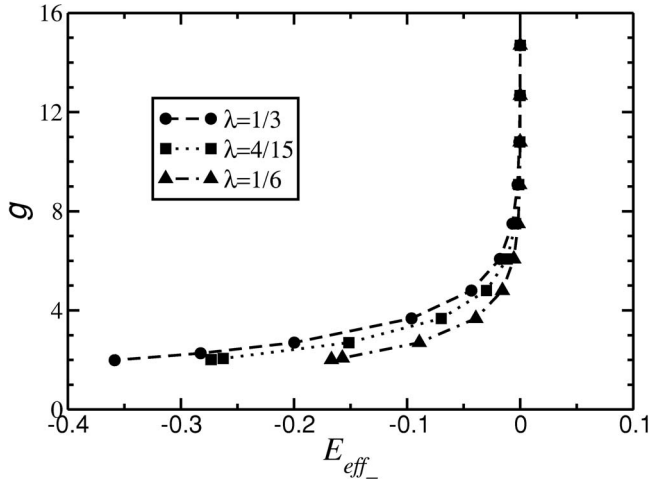

FIG. 2. Mean field phase coexistence curves for $\Lambda_+=0.3$ and $\lambda=\frac{1}{3}$ (circles), $\frac{4}{15}$ (squares), and $\frac{1}{6}$ (triangles). Curves with greater λ shift farther from the $E_{eff\_}$ axis. When g is sufficiently large, all phase coexistence curves shift towards the $E_{eff\_}$ axis; this means that the effect of junction height difference is the dominant mechanism for phase separation at large g.

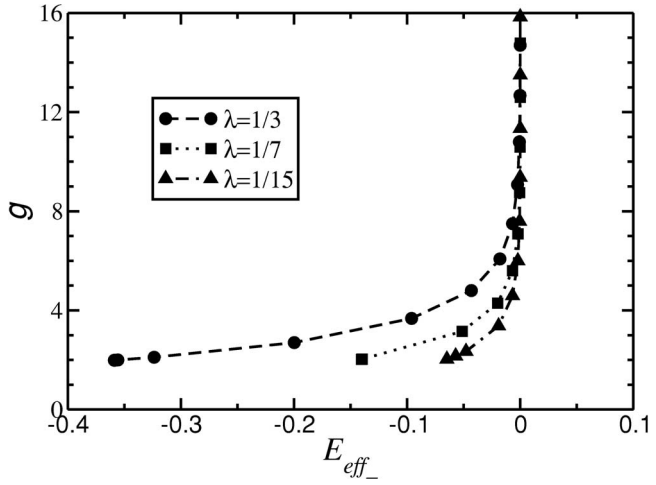

FIG. 3. Mean field phase coexistence curves for $\Lambda_1=0.2$, and $\lambda=\frac{1}{3}$ (circles), $\frac{1}{7}$ (squares), and $\frac{1}{15}$ (triangles). Curves with greater λ shift farther from the $E_{eff\_}$ axis. All phase coexistence curves shift towards the $E_{eff\_}$ axis when g is sufficiently large; this means that the effect of junction height difference is the dominant mechanism for phase separation at large g.

by the height difference of different species of junctions, and it occurs when g is sufficiently large. Along the phase coexistence curve, the system separates into a type-1-junction-rich domain and a type-2-junction-rich domain.

Let us now consider the more general case when different species of junctions have different flexibilities, i.e., $\lambda \neq 0$. In this case, the phase coexistence curve shifts away from $E_{eff\_}=0$. Expanding V_{eff} around $\lambda=0$ leads to the position of the critical point for small λ,

$$g = 2\left(1 - \frac{\lambda^2}{4}\right) + \mathcal{O}(\lambda^4),$$

$$E_{eff-} = -\lambda + \mathcal{O}(\lambda^3). \tag{15}$$

The critical value of g decreases as the difference of junction flexibility increases, and the phase coexistence curve near the critical point shifts away from the $E_{eff\_}$ axis such that $E_{eff\_}$ and λ have opposite signs. We expect that the phase coexistence curves move toward the $E_{eff\_}$ axis as g increases because at large g the effect of junction height difference should be more important than the junction flexibility difference. Since, in this mean field theory, the location of the phase coexistence curve is independent of E_{eff_+}, we plot the phase coexistence curves in two different ways in Figs. 2 and 3. Figure 2 (fixed Λ_+) shows phase boundaries for $\Lambda_+=0.3$ and $\lambda=\frac{1}{3},\frac{4}{15},\frac{1}{6}$, Fig. 3 (fixed λ_1) shows phase boundaries for $\Lambda_1=0.2$ and $\lambda=\frac{1}{3},\frac{1}{7},\frac{1}{15}$. Both figures show that the effect of flexibility difference is indeed more important near the critical point, and at large g the phase boundaries are dominated by junction height difference, therefore they move towards the $E_{eff\_}$ axis as g increases, in agreement with our argument. The critical points agree well with our small λ approximation in Eq. (15) although the shift of g from 2 is too small to be seen from the figures. In this section we only describe the shape of phase boundaries in the mean field theory. The reason that $E_{eff\_}$ and λ have opposite signs near the critical point will be discussed in the next section when Gaussian fluctuations around the mean field solution are included.

It is interesting to point out that in the mean field solution, the sum of the densities of the junctions, $\langle \phi_1 + \phi_2 \rangle$, is the same in both states. This has already been seen in [15] but the reason for this special result can be understood in the effective intermembrane potential approach more clearly. Since

$$\langle \phi_1 + \phi_2 \rangle = \left\langle \frac{\sum_\alpha \exp\left(E_{eff\,\alpha} - \frac{\Lambda_\alpha}{2}(l-l_\alpha)^2\right)}{1 + \sum_\beta \exp\left(E_{eff\,\beta} - \frac{\Lambda_\beta}{2}(l-l_\beta)^2\right)} \right\rangle = 1 - \langle e^{-V_{eff}} \rangle \tag{16}$$

from the fact that in the mean field theory the effective intermembrane potential is the same in both states, therefore the total densities of junctions should be the same in both states. In reality, intermembrane distance fluctuations should be taken into account and this result is only an approximation.

Notice that all the predictions of the mean field theory of this effective intermembrane potential approach are the same as the hard membrane solution of Ref. [15]. In Ref. [15] the hard membrane solution is found by first neglecting membrane height fluctuations, then deriving effective interaction between the junctions. The phase diagram in the hard membrane solution comes from studying the effective interaction between the junctions. Since both approaches neglect fluctuations of intermembrane distance, it is not surprising that they predict the same results on the mean field level. However, it will become clear in the next section that when the

fluctuations of the intermembrane distance are taken into account, the present approach can be applied to study the phase boundary for different E_{eff_+}. On the other hand, the one-loop calculation in Ref. [15] provides the fluctuation-induced interactions between the junctions, but the phase boundary on the one-loop level was not found. The effective membrane theory of Raychaudhuri *et al.* [18] that is derived from the fast-reaction limit of the reaction-diffusion equations of [12] is apparently similar to our theory. However, in Ref. [18] the immunological synapse formation is the main issue, and Raychaudhuri *et al.* mainly study the phase diagram in the $\psi_1\psi_2$ plane for given g, λ, and $E_{B\alpha}$ (these values are taken from the T cell/APC system), while we are interested in the phase diagram on the gE_{eff_-} plane for various values of E_{eff_+} and λ.

IV. FLUCTUATIONS OF INTERMEMBRANE DISTANCE

In the mean field analysis, the equilibrium intermembrane distance is determined by minimizing the effective intermembrane potential and the fluctuations of intermembrane distance are neglected. However, in reality the intermembrane distance is not fixed; instead it fluctuates around the minimums of the effective intermembrane potential. The free energy in a state with average intermembrane distance close to l_α (therefore this minimum is called $l_{min\ \alpha}$) can be calculated approximately by Gaussian approximation, i.e.,

$$\frac{F_\alpha}{k_BT} = -\ln \int \prod_{i,j} dl(i,j) \times \exp\left[-H_{el} - \sum_{i,j} \left(V_{eff} + \frac{V''_{eff}}{2}[l(i,j) - l_{\min\ \alpha}]^2 \right) \right], \tag{17}$$

where V_{eff} and V''_{eff} are both evaluated at $l=l_{min\ \alpha}$. The phase coexistence curve in the Gaussian theory can be determined by comparing the free energies of the two states and seeking the parameters that lead to degenerate free energies. Figure 4 shows the phase boundaries for $E_{eff_+}=2$, $\Lambda_+=0.3$, and $\lambda=\frac{1}{3},\frac{4}{15},\frac{1}{6}$, respectively. Figure 5 shows phase boundaries for systems with $\Lambda_+=0.3$, $\lambda=\frac{1}{3}$, and $E_{eff_+}=-4,-2,2,10$, respectively. Both figures clearly show that the phase coexistence curve has two distinct regions. In the large g region, when $\lambda>0$ ($\lambda<0$), the phase coexistence in the Gaussian theory occurs when $E_{eff_-}>0$ ($E_{eff_-}<0$). In the small g region, the phase boundaries turn towards the opposite side of the E_{eff_-} axis and agree qualitatively with the mean field theory. Figure 4 shows that as λ increases (relative junction flexibility difference increases), the distance between the phase boundary and the E_{eff_-} axis in the large g region becomes more significant. But in the small g region, the phase boundary turns towards the opposite side of the E_{eff_-} axis, and the curvature in the turning region is more significant for systems with greater λ. Figure 5 shows that in the large g region the phase coexistence curves for systems with smaller E_{eff_+} are located farther from the E_{eff_-} axis (the phase boundary predicted by the mean field theory) because fluctuations are more pronounced as E_{eff_+} decreases. On the other hand, the phase boundaries converge towards the same point as g decreases. This is because Gaussian theory predicts the same critical point as mean field theory and in the mean field theory the critical point is independent of E_{eff_+}.

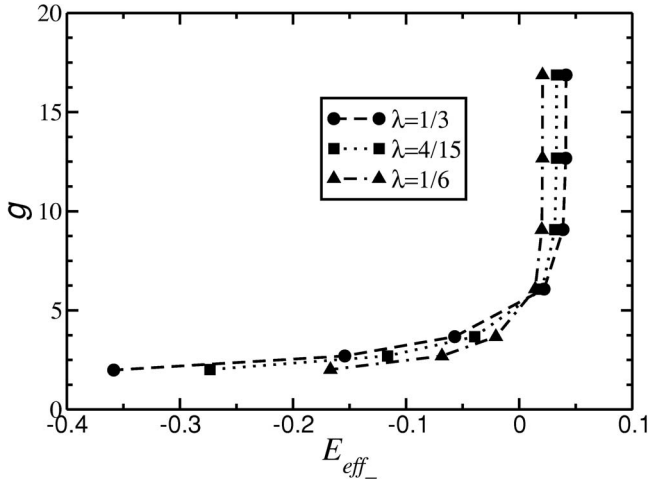

FIG. 4. Phase coexistence curves for $E_{eff_+}=2$, $\Lambda_+=0.3$, and $\lambda=\frac{1}{3}$ (circles), $\frac{4}{15}$ (squares), and $\frac{1}{6}$ (triangles) in Gaussian theory. In the large g region phase coexistence occurs at $E_{eff_-}>0$ and in the small g region phase coexistence occurs at $E_{eff_-}<0$. Phase coexistence curves for systems with greater λ (greater junction flexibility difference) have higher curvature in the crossover region between the large and small g regions.

The shape of the phase boundary in the large and small g regions can be understood by analyzing typical shapes of V_{eff} in both large g and small g regions (plotted in Figs. 6 and 7). Figure 6 shows that $V_{eff}(l_{min\ \alpha})$ and $-\ln(1+e^{-E_{eff\ \alpha}})$ (this ex-

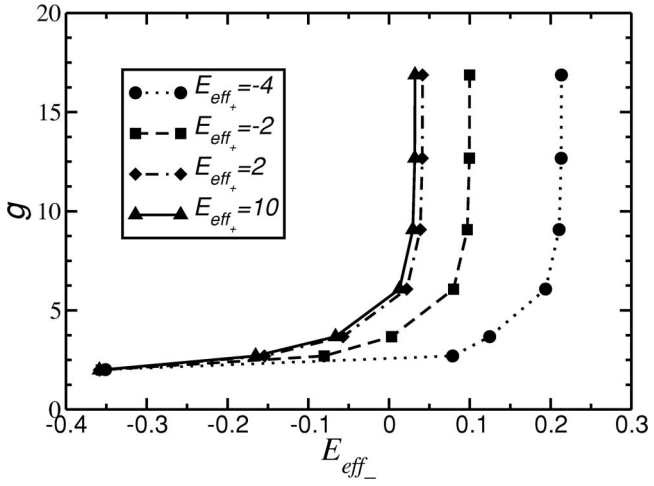

FIG. 5. Phase coexistence curves for $\Lambda_+=0.3$, $\lambda=\frac{1}{3}$, and $E_{eff_+}=-4$ (circles), -2 (squares), 2 (diamonds), and 10 (triangles) in Gaussian theory. In the large g region phase coexistence occurs at $E_{eff_-}>0$ and in the small g region phase coexistence occurs at $E_{eff_-}<0$. Phase coexistence curves for systems with greater E_{eff_+} are closer to the E_{eff_-} axis in the large g region. All curves converge to the same critical point because Gaussian theory predicts the same critical point as the mean field theory and in the mean field theory the critical point is independent of E_{eff_+}.

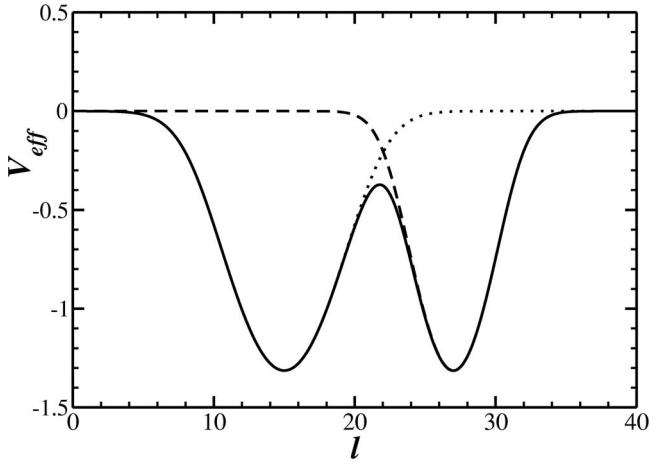

FIG. 6. Effective intermembrane potential in the large g region with $E_{eff_+}=2$, $E_{eff_-}=0$, $\Lambda_+=0.3$, $\lambda=\frac{1}{3}$, and $g=10.8$. The softer junctions are shorter than the harder junctions. Solid curve, V_{eff}; dotted curve, $-\ln\{1+\exp[E_{eff_1}-(\Lambda_1/2)(l-l_1)^2]\}$; dashed curve, $-\ln\{1+\exp[E_{eff_2}-(\Lambda_2/2)(l-l_2)^2]\}$. The dotted and dashed curves almost overlap with the solid curve at l close to l_1 and l_2, respectively. This means that the density of type-α junction in the type-β junction-rich state is negligible. In this case, because the membrane fluctuation around the softer junction is more significant, this state acquires more entropy, therefore phase coexistence should occur when the harder junctions have higher effective binding energy.

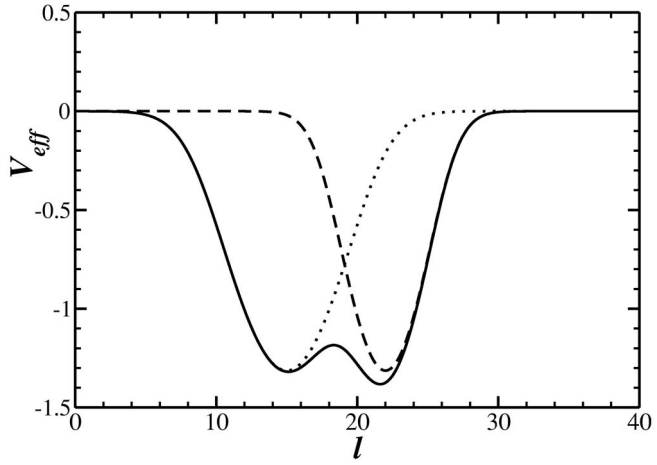

FIG. 7. Effective intermembrane potential in the small g region with $E_{eff_+}=2$, $E_{eff_-}=0$, $\Lambda_+=0.3$, $\lambda=\frac{1}{3}$, and $g=3.675$. The softer junctions are shorter than the harder junctions. Solid curve, V_{eff}; dotted curve, $-\ln\{1+\exp[E_{eff_1}-(\Lambda_1/2)(l-l_1)^2]\}$; dashed curve, $-\ln\{1+\exp[E_{eff_2}-(\Lambda_2/2)(l-l_2)^2]\}$. The dotted curve almost overlaps with the solid curve when l is close to the minimum $l_{min\,1}$, this means that the density of the harder junctions in the domain with l close to the minimum $l_{min\,1}$ is negligible. On the other hand, the dashed curve is considerably higher than the solid curve when l is close to the minimum $l_{min\,2}$, this means that the density of the softer junctions is not negligible in the domain with l close to the minimum $l_{min\,2}$, therefore the effective intermembrane potential at $l_{min\,2}$ is lowered due to the contribution from the binding energy of these softer junctions.

pression is the effective intermembrane potential without contribution of type-β junctions) are very close to each other when l is close to $l_{min\,\alpha}$ for both $\alpha=1$ and 2, therefore in this case the equilibrium density of type-β junctions in a type-α-junction-rich state is negligible ($\beta\neq\alpha$), $l_{min\,\alpha}=l_\alpha$, and the free energy of the type-α-junction-rich state simply comes from the binding energy of type-α junctions and fluctuations of the intermembrane distance around type-α junction's natural height. Due to the higher entropy associated with the softer junctions (more intermembrane distance fluctuations), phase coexistence occurs when the harder junctions have higher effective binding energy (i.e., higher binding energy or higher densities of free ligands and free receptors). This effect is more significant for systems with greater λ (see Fig. 4) or smaller E_{eff_+} (see Fig. 5). On the other hand, in the small g region, the probability that a type-β junction appears in the region where the intermembrane distance is closer to the natural height of type-α junction can be non-negligible. Especially, as Fig. 7 shows, the minimum of V_{eff} at l close to the natural length of the harder junctions is lowered significantly because of the contribution from the binding energy of the softer junctions. Mathematically this can be understood by expanding $V_{eff}(l_{min\,\alpha})$ around small $\exp[E_{eff\,\beta}-(\Lambda_\beta/2)\times(l_{min\,\alpha}-l_\beta)^2]$,

$$V_{eff}(l_{min\,\alpha}) \approx -\ln\left[1+\exp\left(E_{eff\,\alpha}-\frac{\Lambda_\alpha}{2}(l_{min\,\alpha}-l_\alpha)^2\right)\right] - \frac{\exp\left(E_{eff\,\beta}-\frac{\Lambda_\beta}{2}(l_{min\,\alpha}-l_\beta)^2\right)}{1+\exp\left(E_{eff\,\alpha}-\frac{\Lambda_\alpha}{2}(l_{min\,\alpha}-l_\alpha)^2\right)}. \quad (18)$$

The second term on the right-hand side is the contribution from type-β junctions. Thus the minimum of V_{eff} at $l_{min\,\alpha}$ shifts downward due to the presence of β-type junctions, and this shift is more significant when the density of type-β junctions is higher. Clearly, the softer junctions can be stretched or compressed easier than the harder junctions, therefore they are more effective at lowering $V_{eff}(i,j)$ near the minimum closer to the natural length of the harder junctions. Therefore in this case phase boundary shifts towards smaller effective binding energy of the harder junctions.

In the present work the shift of the phase boundary in both large and small g regions finds natural explanation from the shape of effective intermembrane potential while in Ref. [15] only the phase separation near the critical point was explained from the interjunction interaction point of view. In Ref. [15] the phase separation near the critical point was interpreted as the aggregation of the softer junctions since it was shown that the density of the softer junctions near the critical point is higher than the harder junctions in both states, and the phase boundary in the large g region was predicted to be located on the E_{eff_-} axis because junction height difference should be dominant in that region. Therefore the present approach provides the physical mechanisms that control the shape of the phase coexistence curve, and Ref. [15] explains the nature of the phase separation near the mean field critical point. A combination of the both present

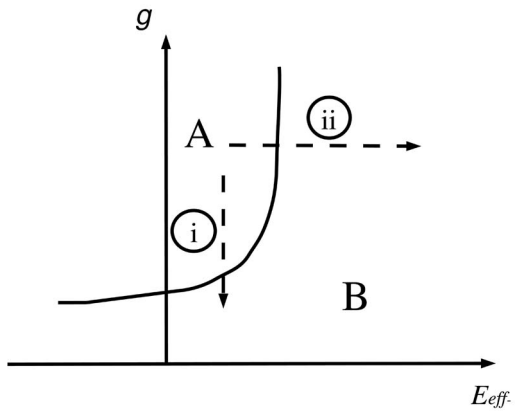

FIG. 8. Schematics of the phase boundary for $\lambda > 0$. There are two routes to move from state A to state B. (i) decrease g and (ii) increase $E_{eff\_}$.

approach and the approach in Ref. [15] provides a complete physical picture of the general adhesion-induced phase separation of two species of junctions.

V. DISCUSSION AND SUMMARY

Through an effective intermembrane potential approach, we have obtained the phase diagram of the systems that we are interested in by mean field and Gaussian theories. Although the phase separation is generally interpreted as driven by the natural height difference of the junctions, we have studied the effects of junction flexibility difference, thermally activated intermembrane distance fluctuations, and the strength of effective binding energy on the phase diagram of these systems, too. The main result of our study is that the dominant physical mechanisms that control the shape of the phase coexistence curve in the $gE_{eff\_}$ plane can be understood by analyzing the shape of the effective intermembrane potential. We find that when different types of junctions have

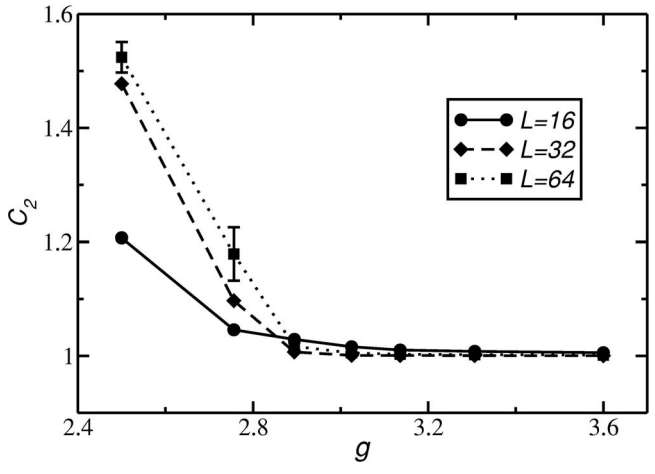

FIG. 9. C_2 as a function of g for $L=16$ (circles), 32 (diamonds), and 64 (squares) for $E_{eff\_}=0$, $\Lambda_+=0.4$, $E_{eff_+}=2$, $\lambda=0$, and $l_1=15$. The common intersection point in this case is close to $g=2.8$. For clarity, error bars are shown for the $L=64$ case only; this is also the case with the greatest error bars.

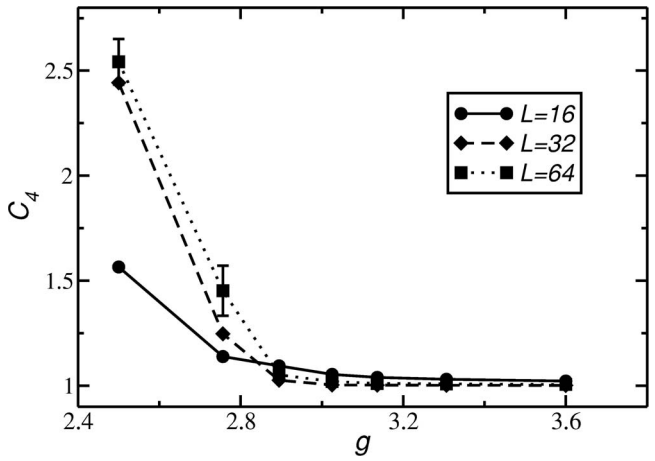

FIG. 10. Binder cumulant C_4 as a function of g for $L=16$ (circles), 32 (diamonds), and 64 (squares) for $E_{eff\_}=0$, $\Lambda_+=0.4$, $E_{eff_+}=2$, $\lambda=0$, and $l_1=15$. The common intersection point in this case is close to $g=2.8$. For clarity, error bars are shown for the $L=64$ case only; this is also the case with the greatest error bars.

different flexibilities, the phase coexistence curve shows very different behavior in the large and small g regions. In the large g region, the fluctuations of intermembrane distance around the natural height of different types of junctions is responsible for the shift of the phase boundary from the $E_{eff\_}$ axis. As a result, phase coexistence occurs when the harder junctions have greater binding energy or higher ligand and receptor densities than the softer junctions. In the small g region, the junction height difference is sufficiently small such that the softer junctions can be stretched or compressed and contribute to the free energy of the state with intermembrane distance close to the natural height of the harder junctions. As a result the effective intermembrane potential at the minimum that is closer to the natural height of the harder junctions is lowered due to the contribution from the binding energy of the softer junctions. This effect makes the phase boundary shift towards the other side of the $E_{eff\_}$ axis where the binding energy of the harder junctions or the densities of ligands and receptors of them are smaller than those of the softer junctions.

Figure 8 shows the schematics of the phase boundary for the case when type-1 junctions are less flexible than type-2 junctions, i.e., $\lambda > 0$. With the wide range of material parameters listed in Table I, in principle the parameter space in Fig. 8 should be able to be explored pretty thoroughly by experiments. However, most of the existing experimental work is carried out in T cell/APC systems, therefore up to now experiments have explored a relatively small region of the parameter space only. To observe a phase transition from state A to state B in Fig. 8 experimentally, one may either (i) reduce the value of g or (ii) increase the value of $E_{eff\_}$. It is relatively difficult to control g during an experiment because $g=(l_1-l_2)^2(\lambda_1-\lambda_2)$, and it is difficult to change either the natural height or the flexibility of the junctions during an experiment. However, the effective binding energy can be tuned by adding free ligands or receptors to the solution, thus a phase transition from state A to state B by method (ii) should be accessible for typical experiments. The dynamics

of this phase transforming process is also an interesting research topic to explore.

Our theory does not include the effects of non-Gaussian fluctuations and the entropic repulsion between the membranes. Non-Gaussian fluctuations should be important near the critical point and the entropic repulsion between the membranes should be important near the unbinding transition. Numerical simulation is a suitable method to study both effects quantitatively; this will be a future work [24]. Here we first discuss the effect of non-Gaussian fluctuations on the critical point of our systems. It is well known that the critical value of g, i.e., g_c, is located at higher g than the prediction of the mean field theory, and the actual value of g_c should depend on surface tension, membrane bending rigidity, and E_{eff_+} (i.e., the binding energies of the junctions and the densities of the ligands and receptors), therefore it remains to check whether the small g region discussed in this article can actually be observed in typical systems. The Monte Carlo simulations discussed in the Appendix suggest that the phase separation in the small g region should be able to be observed in typical systems. However, it is still possible there are some special cases where E_{eff_+} can be extremely small such that small g region of the phase coexistence may not be observed because g_c in these systems becomes very large. We further point out that the mechanisms that control the shape of the phase boundaries mentioned in this article come from observing the shape of V_{eff}. Therefore they are not affected qualitatively by the approximations made in our calculations. We expect non-Gaussian fluctuations change the exact location of phase coexistence curves, but the qualitative shape of these curves should be the same as our prediction.

In summary, the phase diagram of membrane-adhesion-induced phase separation of two species of junctions is studied thoroughly with mean field and Gaussian theories. Our study reveals the physics behind this phase diagram as long as the system is not too close to the unbinding transition where membrane-membrane collisions are important. The result of our study can be useful for designing biomimetic membrane systems and in studying cell adhesion processes. The adhesion and detachment dynamics for these systems is an important problem that remains partially understood [12,14,25], and our study could be a suitable starting point for future research work in this direction.

ACKNOWLEDGMENTS

This work is supported by the National Science Council of the Republic of China (Taiwan) under Grant No. NSC 93-2112-M-008-030. H.-Y.C. thanks the National Center for Theoretical Sciences (Hsinchu) for the hospitality and financial support during his visit, where part of this work was done.

APPENDIX

In this appendix we present some preliminary results from the Monte Carlo simulations applied to our systems. The simulations are performed on lattices with size up to 128 $\times 128$ sites for $\lambda=0$ (both types of junctions have the same flexibility), $E_{eff_-}=0$, $\Lambda_+=0.4$ (corresponds to typical systems), $l_1=15$, $-4 \leqslant E_{eff_+} \leqslant 8$, and different values of g. Simulations for $\lambda \neq 0$ (junctions have different flexibilities) and $E_{eff_+} < -4$ (very weak effective binding energy, near unbinding transition) will be reported in a future work [24]. Metropolis algorithm and periodic boundary conditions are applied to the simulations. To determine the critical point, we define the Binder cumulants C_2 and C_4,

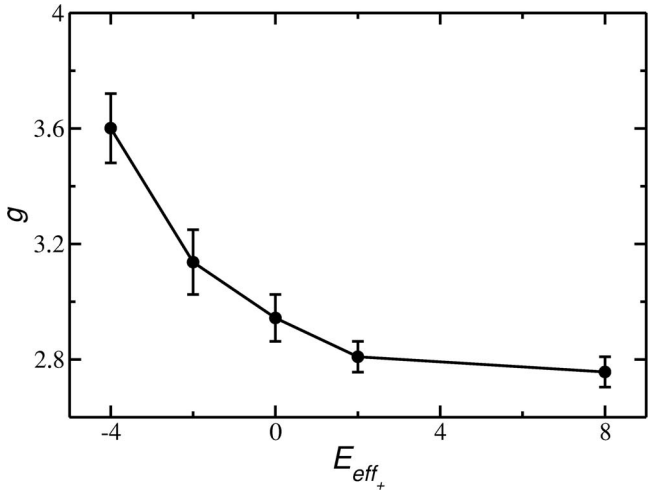

FIG. 11. g_c as a function of E_{eff_+} for $E_{eff_-}=0$, $\Lambda_+=0.4$ (corresponds to typical systems), $\lambda=0$, and $l_1=15$. g_c increases as E_{eff_+} decreases; for E_{eff_+} between -4 and 8 the value of g_c for $\lambda=0$ varies from 3.6 to 2.8.

$$C_2 = \frac{\langle \bar{z}^2 \rangle}{\langle |\bar{z}| \rangle^2}, \quad C_4 = \frac{\langle \bar{z}^4 \rangle}{\langle \bar{z}^2 \rangle^2}, \tag{A1}$$

where

$$\bar{z} = \frac{1}{N} \sum_{i,j}^{L} z(i,j) \tag{A2}$$

is the spatial average of z. For $g > g_c$ and $L \gg \xi$ (the correlation length of z), the moments reach the values $C_2=1$ and $C_4=1$. For $0 < g < g_c$ and $L \gg \xi$, $C_2=\pi/2$ and $C_4=3$. For $0 < g < g_c$ and $L \ll \xi$, C_2 and C_4 vary only weakly with the linear size L [23,26]. Therefore g_c can be found from the common intersection point of C_2 and C_4, respectively, as functions of g for several values of L [23,26].

Figures 9 and 10 show C_2 and C_4 for $E_{eff_-}=0$, $E_{eff_+}=2$, $\Lambda_+=0.4$, $l_1=15$, and several values of L. In this case the critical point is located at $g_c \approx 2.8$. The critical points for different E_{eff_+} are determined in this way and shown in Fig. 11. It is clear that g_c increases as E_{eff_+} decreases, as we expected. Figure 11 shows that for E_{eff_+} between -4 and 8

the value of g_c for $\lambda=0$ varies from 3.6 to 2.8. At least for small λ, we expect g_c for typical systems also falls within similar range. Since Figs. 4 and 5 both show that the crossover from large g region to small g region occurs at $g \geqslant 6$, we conclude that small g region can be observed in typical systems. However, it is possible that in certain special cases, E_{eff_+} can be very small and small g region of phase coexistence could not be observed in these systems.

[1] R. Lipowsky and E. Sackmann, *The Structure and Dynamics of Membranes* (Elsevier, Amsterdam, 1995).

[2] H. Strey, M. Peterson, and E. Sackmann, Biophys. J. **69**, 478 (1995).

[3] A. Albersdörfer, T. Feder, and E. Sackmann, Biophys. J. **73**, 245 (1997).

[4] J. Nardi, T. Feder, and E. Sackmann, Europhys. Lett. **37**, 371 (1997).

[5] R. Bruinsma, A. Behrisch, and E. Sackmann, Phys. Rev. E **61**, 4253 (2000).

[6] T. R. Weikl, R. R. Netz, and R. Lipowsky, Phys. Rev. E **62**, R45 (2000).

[7] T. R. Weikl and R. Lipowsky, Phys. Rev. E **64**, 011903 (2001).

[8] S. Komura and D. Andelman, Eur. Phys. J. E **3**, 259 (2000).

[9] D. Zuckerman and R. Bruinsma, Phys. Rev. Lett. **74**, 3900 (1995).

[10] T. R. Weikl, J. T. Groves, and R. Lipowsky, Europhys. Lett. **59**, 916 (2002).

[11] C. R. F. Monks *et al.*, Nature (London) **395**, 82 (1998); G. Grakoui *et al.*, Science **285**, 221 (1999); D. M. Davis *et al.*, Proc. Natl. Acad. Sci. U.S.A. **96**, 15062 (1999).

[12] S. Y. Qi, J. T. Groves, and A. K. Chakraborty, Proc. Natl. Acad. Sci. U.S.A. **98**, 6548 (2001).

[13] N. J. Burroughs and C. Wülfing, Biophys. J. **83**, 1784 (2002).

[14] T. R. Weikl and R. Lipowsky, Biophys. J. **87**, 3665 (2004).

[15] H.-Y. Chen, Phys. Rev. E **67**, 031919 (2003).

[16] D. Coombs, M. Dembo, C. Wofsy, and B. Goldstein, Biophys. J. **86**, 1408 (2004).

[17] G. I. Bell, M. Dembo, and P. Bongrand, Biophys. J. **45**, 1051 (1984).

[18] S. Raychaudhuri, A. K. Chakraborty, and M. Kardar, Phys. Rev. Lett. **91**, 208101 (2003).

[19] Apparently, therefore, our theory does not consider the case when junction densities are higher than one junction per lattice site (area a^2). This extremely high density may occur when, for example, receptor clustering happens, but in those cases the direct interactions between the ligands and receptors cannot be neglected either.

[20] R. Lipowsky, Phys. Rev. Lett. **77**, 1652 (1996).

[21] D. Needham and R. M. Hochmuth, Biophys. J. **61**, 1664 (1992).

[22] R. Goetz, G. Gompper, and R. Lipowsky, Phys. Rev. Lett. **82**, 221 (1999).

[23] T. R. Weikl, D. Andelman, S. Komura, and R. Lipowsky, Eur. Phys. J. E **8**, 59 (2002).

[24] J.-Y. Wu and H.-Y. Chen (unpublished).

[25] Notice that the detachment process is not studied in either Ref. [12] or [14]. They both study the adhesion dynamics only.

[26] K. Binder and D. W. Heermann, *Monte Carlo Simulations in Statistical Physics* (Springer, Berlin, 1992).